IOSR Journal of Engineering (IOSRJEN) **www.iosrjen.org**
ISSN (e): 2250-3021, ISSN (p): 2278-8719
Vol. 09, Issue 8 (August. 2019), ||S (I) || PP 40-43

Nonlinear PWM-Controlled Photovoltaic Inverter with Reduced Number of Switches

Mulagiri Madhu Babu[1] G Ramudu[2]
[1]PG Scholar, Dept.of EEE, Chirala Engineering College, chirala, India.
[2]AssistantProfessor, Dept.of EEE, Chirala Engineering College, India

Abstract: A nonlinear pulse width modulation-controlled single-phase boostmode photovoltaic grid-connected inverter with limited storage inductance current is proposed in this paper. The circuit topology, control strategy, steady-state principle characteristic, and design criterion for the key circuit parameters of this kind of inverter are investigated in depth, and important conclusions are obtained. The inverter's regenerating energy duty ratio 1–D which decreases with the decline of the grid-connected voltage is real time adapted by sampling and feeding back the inverting bridge modulation current, and the average value of the modulation current in each switching cycle tracks the reference sinusoidal signal to get high-quality grid-connected current. The active control of the energy storage inductance current and the balance of the voltage step-up ratio are realized by adding a bypass switch connected inparallel with the energy storage inductance and using two kinds of switching pattern namely boost pattern and freewheeling pattern.

Index Terms: Boostmode, limitedstorageinductancecurrent, nonlinear pulse width modulation (PWM) control, photovoltaic (PV) grid-connected inverter, single-phase.

Date of Submission: 03-08-2019 Date of Acceptance: 19-08-2019

I. INTRODUCTION

THE single stage inverter has become a research hotspot in the new energy power-generating field [1]–[8]. Compared with the buck mode inverter, the boost mode inverter has the advantages of single-stage voltage boosting, direct control of the output current and easy realizing the maximum power point tracking (MPPT) of the photovoltaic (PV) cell, long life of the energy storage inductors' components, timely protection with over current and high system reliability, etc. In recent years, with the emergence of new type devices such as bidirectional blocking insulated-gate bipolar transistor (IGBT) and the development of superconducting technology, boost mode inverter will have a more important application value.

Based on the derived nonlinear modulation compensation function restraining harmonic waves of the grid-connected current, the proposed control strategy, respectively, extracts the dc and ac components of the energy storage inductance current and compares with the grid-connected current reference to get the nonlinear PWM signal which can inhibit third harmonic wave of the grid-connected current. The proposed control strategy can effectively suppress the third harmonic wave of the grid-connected current, but there still are defects such as large energy storage inductance (21 mH) and THD of the output current waveform up to 4.42%. A control strategy based on the inverter's output current involving feedforward and feedback terms is proposed, which improves the quality of output waveforms, but the energy storage inductance *L* is still as high as 10 mH; the conversion efficiency and THD of the output voltage are not given. A parallel resonator is connected in series between the input source and energy storage inductor of the traditional inverter, and an output voltage and current feedback control strategy with proportional resonant is adopted. The parallel resonator can filter out the second and fourth low-frequency harmonic component in energy storage inductor current and reduce the energy storage inductor and the input low-frequency ripple to some extent. The control strategy effectively improves the quality of output waveform, but the resonant inductors in the parallel resonator are high up to 5 and 10 mH and the energy storage inductor value of the inverter is 5 mH. Only light-load waveform is provided and the conversion efficiency is not provided. To overcome inherent defects of the traditional single-phase boost mode inverter, a nonlinear PWM-controlled single-phase boost mode PV grid-connected inverter with limited energy storage inductance current is proposed and deeply researched in this paper, and important conclusions are obtained.

II. NONLINEAR PWM CONTROL STRATEGY

Control Principle

In order to improve the quality of output waveform of the traditional single-phase boost mode inverter, a new idea that regenerating duty ratio 1–*D* of the inverter decreases with the decline of the grid-connected voltage *un* , namely a nonlinear

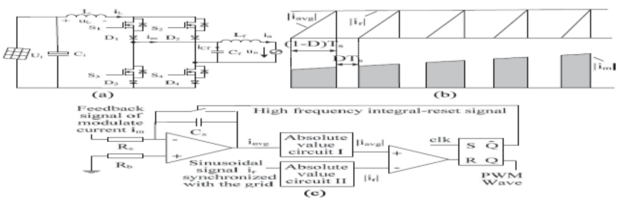

Fig. 1. Circuit topology of traditional single-phase boost mode inverter and nonlinear PWM control strategy. (a) Circuit topology. (b) Control principle waveform. (c) Control circuit block.

PWM control strategy based on inverting bridge's modulation current is proposed in this paper, as shown in Fig. 1. This control strategy is that the inverter's regenerating energy duty ratio 1–*D* is real time regulated by detecting and feeding back the modulation current *i*m and high-quality grid-connected current is obtained. When the grid voltage *un* is less than the input voltage *Ui*, *im* is greater than the expected value and the integral time (1–*D*) *Ts* of the feedback signal *im* to the reference value |*ir* | will become shorter, 1–*D* will be decreased; thus, the waveform quality of the grid-connected current *in* will be improved.Set the switching period is *Ts* , and the integral circuit's time constant is *RsCs* = *Ts* . After the modulation current feedback signal *im* of the inverter through the integral circuit and the absolute value circuit, the average value *i*avg of *im* is obtained, and its absolute value |*i*avg | can be derived as follows:

$$|i_{avg}| = \frac{1}{R_s C_s}\left|\int_0^{(1-D)T_s} i_m \mathrm{dt}\right| = \frac{1}{T_s}\left|\int_0^{(1-D)T_s} i_m \mathrm{dt}\right|. \quad (1)$$

The average value of harmonic current in *C*f within one *Ts* is zero; thus, the average value of output filtering capacitance current *iCf* within one *Ts* is the average value of its fundamental wave component *iCf*1 , namely

$$\frac{1}{T_s}\int_0^{(1-D)T_s} i_m \mathrm{dt} = \frac{1}{T_s}\int_0^{T_s} i_{Cf1} \mathrm{dt} + \frac{1}{T_s}\int_0^{T_s} i_n \mathrm{dt} \overset{\text{most range of load}}{\approx} \frac{1}{T_s}\int_0^{T_s} i_n \mathrm{dt}. \quad (2)$$

Equations (1) and (2) show that the average value of *in* approximately equals to *i*avg within one *Ts* . Therefore, *in* can be controlled by controlling the reference signal *ir* . When *Ui* changes, the constant of *in* is realized by adjusting 1–*D*. As *im* is nearly constant during (1–*D*) *Ts* , derived from (1)

$$|i_m(1 - D)| = |i_{\mathrm{avg}}| = |i_r|.$$

$$1 - D = |i_r / i_m|.$$

Equation (4) shows that 1–*D* is proportional to |*ir /im*| and is not proportional to the error current *ir* − *im*. Therefore, the control strategy is called nonlinear PWM control strategy.

III. STEADY PRINCIPLE CHARACTERISTICS

A. Equivalent Circuit and Operating Modes in Low Frequency (LF) Output Period

According to the relative value *un/Ui* , the inverter's switching pattern I or II, and the polarity of the modulation current *im*, the proposed inverter has six kinds of equivalent circuits and A, B, C, D, E, F six operating modes within a LF output period (*t*0–*t*8), as shown in Fig. 4 and Table I.

B. Operating Principle of Intervals

There are eight operating intervals for the inverter within an LF output period (*t*0–*t*8), as shown in Fig. 2(g). [*t*0–*t*1]: 0 < *un* < *Ui* , operating inMode A. *L* is freewheeling during *DTs* and magnetizing during (1–*D*) *Ts* . *iL* keeps rising, *iL* > *IL* *. The inverter operates in switching pattern II corresponding to the equivalent circuit, as shown in Fig. 2(e) and (c). Since 1–*D* is quiet small around *un* 's zero point, *iL* rises slowly. *un* rises to the *Ui* and *iL* reaches its maximum value *iL*max at the time *t*1 .

$$\begin{aligned} i_{L\max} &= \sum_{k=-\alpha f_s/\omega}^{\alpha f_s/\omega} \frac{U_i - \sqrt{2}U_n\,|\sin(\omega k T_s)|}{L}[1 - D(k)]T_s + I_L^* \\ &= \int_{-\alpha f_s/\omega}^{\alpha f_s/\omega} \frac{U_i - \sqrt{2}U_n\,|\sin(\omega t)|}{L}\,\frac{U_i}{\sqrt{2}U_n}\,|\sin(\omega t)|\,dt + I_L^* \\ &= \frac{U_i}{\sqrt{2}U_n\omega L}\left[2U_i(1 - \cos\alpha) + \frac{U_n(\sin 2\alpha - 2\alpha)}{\sqrt{2}}\right] + I_L^*. \end{aligned}$$

The angle *α* is the corresponding angle when *un* = *Ui* , namely

$$\alpha = \omega(t_1 - t_0) = \arcsin\frac{U_i}{\sqrt{2}U_n}.$$

[*t*1–*t*2]: *un* > *Ui* , operating in Mode B. L is freewheeling during *DTs* and demagnetizing during (1–*D*) *Ts* . *iL* > *IL* *, the inverter operates in switching pattern II corresponding to the equivalent circuit, as shown in Fig. 2(e) and (c). After every *Ts* period, *iL* is always higher than *IL* * and decreasing, 1–*D* is increasing, and the drop rate of *iL* is increasing. At moment *t*2, *iL* rapidly drops back within *IL* *. The angle *β* is the corresponding angle of *iL* from the maximum value at *t*1 to within *IL* * at *t*2 , namely *β* = *ω*(*t*2 −*t*1). Set *iL* (*t*2) = *IL* *, since the decline value of *iL* from *t*1 to *t*2 is equal to the difference between *iL*max and *IL* *, derived as

$$\begin{aligned} &\sum_{k=-\alpha f_s/\omega}^{\alpha f_s/\omega} \frac{U_i - \sqrt{2}U_n\,|\sin(\omega k T_s)|}{L}\,\frac{U_i}{\sqrt{2}U_n}\,|\sin(\omega k T_s)|\,T_s \\ &= \sum_{k=\alpha f_s/\omega}^{(\alpha+\beta)f_s/\omega} \frac{\sqrt{2}U_n\sin(\omega k T_s) - U_i}{L}\,\frac{U_i}{\sqrt{2}U_n}\sin(\omega k T_s)T_s. \quad (\end{aligned}$$

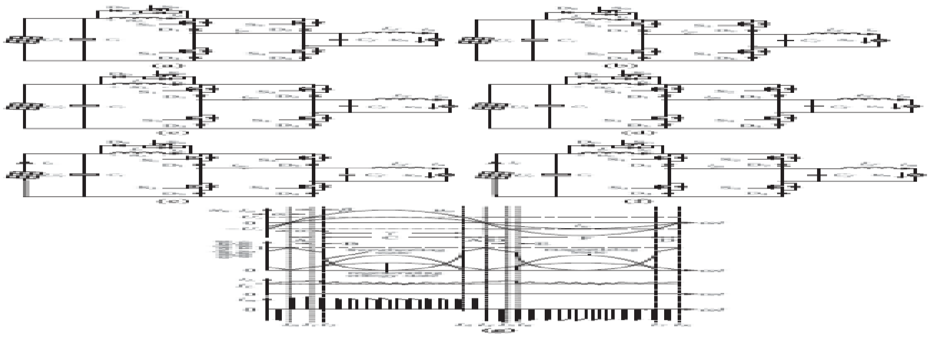

Fig. 2. Equivalent circuit and steady principle waveform of the inverter. (a) Magnetizing state for *im* > 0. (b) Magnetizing state for *im* < 0. (c) Regenerating energy state for *im* > 0. (d) Regenerating energy state for *im* < 0. (e) Freewheeling state for *im* > 0. (f) Freewheeling state for *im* < 0. (g) Steady principle waveform within a LF output period.

[*t*2–*t*3]: *un* > *Ui* , operating inMode C. *iL* is in HF pulsing state around *IL* ∗, and switching patterns I and II operate alternately. If *iL* < *IL* ∗ and the inverter operates in switching pattern I, *L* is magnetizing during *DTs* and demagnetizing during (1–*D*) *Ts, iL* is increasing, if *iL* > *I*∗*L* , the inverter operates in switching pattern II, *L* is freewheeling during *DTs* and demagnetizing during (1–*D*) *Ts, iL* is decreasing. Set from the *k*th *Ts*, the inverter continuously operates in switching mode I for*m*of *Ts* , and from(*k*+*m*)th *T*s , the inverter continuously operates in switching mode II for *n* of *Ts*, . . . in one *T*es , *m* and *n* are natural number, then *iL* is back within *IL* ∗ again, the current variation of *L* can be approximately considered as zero, namely

$$\sum_{j=k}^{k+m-1} \frac{U_i}{L} D(j) T_s + \sum_{j=k}^{k+m+n-1} \frac{U_i - |u_n|}{L} [1 - D(j)] T_s = 0.$$

TABLE I
SIX OPERATING MODES IN ONE LF PERIOD

Operating mode	Corresponding interval	Comparing u_n with U_i	Changing law of i_L	Switching pattern
A	$t_0 - t_1$, $t_3 - t_4$	$0 < u_n < U_i$	$i_L > I_L *$ and increasing	II
B	$t_1 - t_2$	$u_n > U_i$	$i_L > I_L *$ and decreasing	II
C	$t_2 - t_3$	$u_n > U_i$	HF pulsing around $I_L *$	Alternating of I, II
D	$t_4 - t_5$, $t_7 - t_8$	$0 > u_n > -U_i$	$i_L > I_L *$ and increasing	II
E	$t_5 - t_6$	$u_n < -U_i$	$i_L > I_L *$ and decreasing	II
F	$t_6 - t_7$	$u_n < -U_i$	HF pulsingaround $I_L *$	Alternating of I, II

Combination (13) with (18), the equivalent duty ratios of magnetizing and freewheeling states during each *T*es , respectively, are

$$\sum_{j=k}^{k+m-1} \frac{D(j)}{m+n} = \sin^2(\omega t) - \frac{U_i}{\sqrt{2} U_n} \sin(\omega t)$$
$$\sum_{j=k+m}^{k+m+n-1} \frac{D(j)}{m+n} = \cos^2(\omega t).$$

The equivalent duty ratio of regenerating energy state during each *T*es meets (13). The corresponding equivalent circuits of the three kinds of state for this interval are shown in Fig. 2(a), (e), and (c). The angle *γ* is the corresponding angle from *iL* first dropping to *IL* ∗at *t*2 to *un* decreasing to *Ui* at *t*3 , namely

$$\gamma = \pi - 2\alpha - \beta.$$

[*t*3–*t*4]: 0 < *un* < *Ui* , operating in Mode A. The operating principle is the same with that of the interval [*t*0–*t*1]. The angle *α* is the corresponding angle when *un* is decreasing from *Ui* to 0.

[*t*4–*t*5]: 0 > *un* > −*Ui* , operating in Mode D. The corresponding equivalent circuits are shown in Fig. 4(f) and (d). The operating principle is the same with that of the interval [*t*0–*t*1].

[*t*5–*t*6]: *un* < −*Ui* , operating in Mode E. The corresponding equivalent circuits are the same with those of Mode D. The operating principle is the same with that of the interval [*t*1–*t*2].

[*t*6–*t*7]: *un* < −*Ui* , operating in Mode F. The corresponding equivalent circuits are shown in Fig. 4(b), (f), and (d). The operating principle is the same with that of the interval [*t*2–*t*3].

[*t*7–*t*8]: 0 > *un* > −*Ui* , operating in Mode D.The operating principle is the same with that of the interval [*t*4–*t*5].It can be seen that the LF operating modes' sequence of the inverter is A–B–C–A–D–E–F–D.In addition, the current *iS*0 through *S*0 under the freewheeling state is the energy storage inductor current *iL* . If the HF switch current component is ignored and approximately consider *iL* = *IL* ∗, *iS*0 is derived from (12) and (20) at the normal voltage boosting interval corresponding to operating Modes C and F

$$i_{S0} = 2P_n \cos^2(\omega t)/U_i = P_n[1 - \cos(2\omega t)]/U_i.$$

The previous equation shows that the double line frequency component of the input-side current of the inverting bridge mainly flows through $S0$; thus, the energy storage inductor of
the inverter can be greatly reduced.

IV. SIMULATION RESULTS

Designed example: input dc voltage Ui = 98 −122V, grid voltage Un = 220V 50 Hz, rated power P = 1kW, the switching frequency fs = 50 kHz, current sampling frequency selected for 50 kHz, energy storage inductor L = 1mH, input filtering capacitor $Ci = 3 \times 1800\ \mu$F, output filtering capacitor $Cf = 9\mu$F, output filtering inductor Lf = 0.5mH.

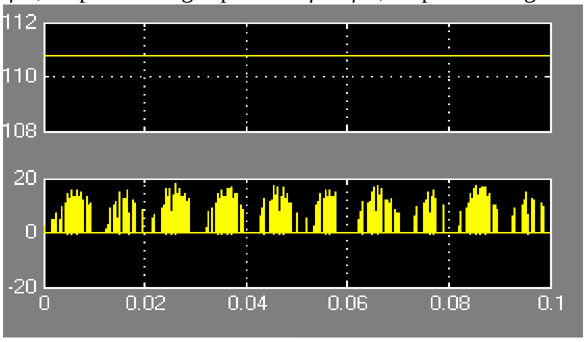

Fig.3. Vpv and Ipv

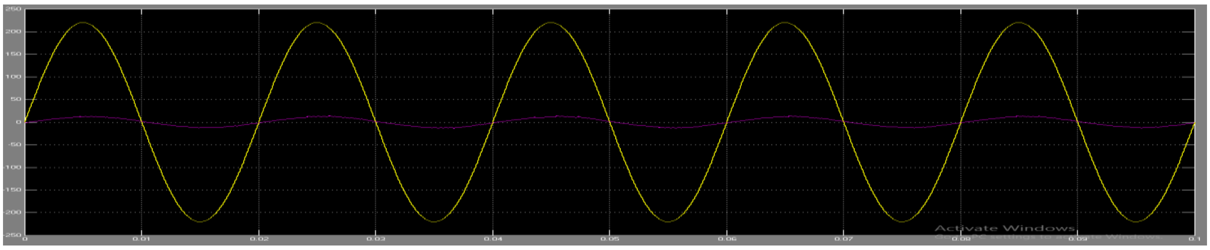

Fig.4. Grid voltage and Grid current

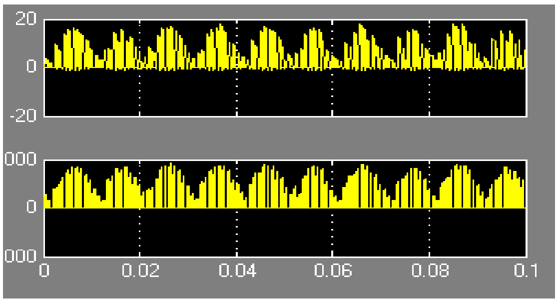

Fig.5. Voltage and current across switch 0.

V. CONCLUSION

1) A nonlinear PWM control strategy based on inverting bridge modulation current is proposed. The size of 1–D is timely adjusted by detecting and feeding back modulation current im, and the quality of output waveform is improved.
2) A circuit topology of the single-phase boost mode gridconnected inverter with additional bypass switch of the energy storage inductor and two types of switching pattern with limitation current of the energy storage inductor is proposed. The active control of the energy storage inductor current is realized by the freewheeling state of energy storage inductor replacing the magnetizing state. The problems such as excess energy of the energy storage inductor and too large step-up ratio of the inverter can be effectively solved and the conversion efficiency is also improved.

REFERENCES

[1]. M. K. Nguyen, T. V. Le, S. J. Park, and Y. C. Lim, "A class of quasiswitched boost inverters," *IEEE Trans. Ind. Electron.*, vol. 62, no. 3, pp. 1526–1536, Jul. 2015.
[2]. S. S. Nag and S. Mishra, "Current-fed switched inverter," *IEEE Trans. Ind. Electron.*, vol. 61, no. 9, pp. 4680–4690, Nov. 2014.
[3]. B. Singh, C. Jain, and S. Goel, "ILST control algorithm of single-stage dual purpose grid connected solar PV system," *IEEE Trans. Power Electron.*, vol. 29, no. 10, pp. 5347–5357, Dec. 2014.
[4]. Y. Tang, X. Dong, and Y. He, "Active buck-boost inverter," *IEEE Trans. Ind. Electron.*, vol. 61, no. 9, pp. 4691–4697, Dec. 2014.
[5]. J.R. Espinoza and G. Joos, "Acurrent-source-inverter-fed inductionmotor drive system with reduced losses," *IEEE Trans. Ind. Appl.*, vol. 34, no. 4, pp. 796–805, Aug. 1998.